ORIGINAL RESEARCH

Cigarette Smoke Disrupted Lung Endothelial Barrier Integrity and Increased Susceptibility to Acute Lung Injury via Histone Deacetylase 6

Diana Borgas, Eboni Chambers, Julie Newton, Junsuk Ko, Stephanie Rivera, Sharon Rounds, and Qing Lu

Vascular Research Laboratory, Providence Veterans Affairs Medical Center, Department of Medicine, Alpert Medical School of Brown University, Providence, Rhode Island

Abstract

Epidemiologic evidence indicates that cigarette smoke (CS) is associated with the development of acute lung injury (ALI). We have previously shown that brief CS exposure exacerbates lipopolysaccharide (LPS)-induced ALI *in vivo* and endothelial barrier dysfunction *in vitro*. In this study, we found that CS also exacerbated *Pseudomonas*-induced ALI in mice. We demonstrated that lung microvascular endothelial cells (ECs) isolated from mice exposed to CS had a greater permeability or incomplete recovery after challenges by LPS and thrombin. Histone deacetylase (HDAC) 6 deacetylates proteins essential for maintenance of endothelial barrier function. We found that HDAC6 phosphorylation at serine-22 was increased in lung tissues of mice exposed to CS and in lung ECs exposed to cigarette smoke extract (CSE). Inhibition of HDAC6 attenuated CSE-induced increases in EC permeability and CS priming of ALI. Similar barrier protection was provided by the microtubule stabilizer taxol, which preserved α-tubulin acetylation. CSE decreased α-tubulin acetylation and caused microtubule depolymerization. In coordination with increased HDAC6 phosphorylation, CSE inhibited Akt and activated glycogen synthase kinase (GSK)-3β; these effects were ameliorated by the antioxidant N-acetyl cysteine. Our results suggest that CS increases lung EC permeability, thereby enhancing susceptibility to ALI, likely through oxidative stress–induced Akt inactivation and subsequent GSK-3β activation. Activated GSK-3β may activate HDAC6 via phosphorylation of serine-22, leading to α-tubulin deacetylation and microtubule disassembly. Inhibition of HDAC6 may be a novel therapeutic option for ALI in cigarette smokers.

Keywords: cigarette smoke; acute lung injury; endothelial cells; permeability; histone deacetylase 6

Clinical Relevance

Epidemiologic and animal studies have indicated that cigarette smoking increases the risk of acute lung injury (ALI). However, the contribution of lung endothelial cells (ECs) and underlying mechanism are unknown. This study demonstrates that cigarette smoke (CS) exposure alters histone deacetylase (HDAC) 6 signaling in lung ECs and that inhibition of this signaling pathway protects against CS exacerbation of ALI and endothelial permeability. These data suggest that inhibition of HDAC6 may be a novel therapeutic option for ALI in cigarette smokers.

More than 20 million Americans died prematurely as a result of cigarette smoke (CS)–induced diseases in the last 50 years (1). In addition to causing chronic obstructive pulmonary disease (COPD) and lung cancer, and increasing risk of heart failure, stroke, and peripheral vascular disease, CS also predisposes lungs to infections by viruses (2) and bacteria (3–5). Growing epidemiological evidence indicates that CS also increases susceptibility to the development of acute lung injury (ALI) and

(Received in original form May 4, 2015; accepted in final form September 28, 2015)

This work was supported by the use of facilities at the Providence Veterans Affairs (VA) Medical Center and by an Institutional Development Award from the National Institute of General Medical Sciences of the National Institutes of Health under grant P20GM103652 (Q.L., project 1), P20GM103652 (S. Rounds), VA Merit Review (S. Rounds), American Thoracic Society/Pulmonary Hypertension Association research grant PH05015 (Q.L.), R25 HL088992 (S. Rivera), and T32 ES007272 (E.C.).

Author Contributions: Conception and design—D.B., S. Rounds, and Q.L.; acquisition and analysis of data—D.B., E.C., J.N., J.K., S. Rivera, and Q.L.; data interpretation—D.B. and Q.L.; drafting the manuscript—Q.L.; revision of the manuscript—D.B., S. Rounds, and Q.L..

Correspondence and requests for reprints should be addressed to Qing Lu, D.V.M., Ph.D., Providence Veterans Affairs Medical Center, Research Services, 830 Chalkstone Avenue, Providence, RI 02908. E-mail: qing_lu@brown.edu

This article has an online supplement, which is accessible from this issue's table of contents at www.atsjournals.org

Am J Respir Cell Mol Biol Vol 54, Iss 5, pp 683–696, May 2016

Originally Published in Press as DOI: 10.1165/rcmb.2015-0149OC on October 9, 2015
Internet address: www.atsjournals.org

acute respiratory distress syndrome (ARDS) in critically ill patients with trauma or nonpulmonary sepsis (6–9). Active CS also increases susceptibility to ARDS even in younger, healthier patients (7). A multicenter cohort study of 8,962 patients in Australia and New Zealand reported that smoking has a dose-related adverse effect on mortality in critically ill patients after adjusting for other confounders (10). Compared with nonsmokers, smokers had a longer intensive care unit stay and a higher risk of requiring mechanical ventilation and dying in hospital (10). ALI and ARDS are characterized by lung inflammation and loss of alveolar endothelial and epithelial barrier integrity. It is well known that CS causes lung inflammation (11–13) and increases alveolar epithelial permeability (14–16) in human and animal models. Lung inflammation and alveolar epithelial cell injury has been shown to contribute to CS-primed mechanical ventilation–induced ALI in rats (17). However, the effect of CS on pulmonary circulation, particularly lung endothelial cells (ECs), is less clearly documented. Chronic CS exposure causes pulmonary endothelial dysfunction in otherwise healthy young smokers (18) and guinea pigs (19, 20). The injurious effect of CS on pulmonary endothelium has been implicated in the development of pulmonary artery hypertension in patients with COPD (21, 22). Pulmonary endothelial denudation has also been documented in chronic smokers with COPD (23). We and others have previously shown that CS increases cultured lung endothelial monolayer permeability *in vitro* (24–26) and promotes lung vascular permeability in mice (25). Increased vascular permeability was also reported in myocardial capillaries of rats exposed to CS (27). However, the mechanism(s) of CS impact on lung ECs is not well understood.

Endothelial barrier integrity is regulated by the dynamic opening and closure of intercellular adherens junctions (AJs) (28, 29) and dynamics of F-actin cytoskeleton and microtubules (30). Tyrosine (Tyr) phosphorylation of two major components of AJs, vascular endothelial (VE)-cadherin and β-catenin, is recognized as an important mechanism of increased endothelial permeability by promoting AJ disassembly (28, 31). β-catenin deacetylation has also been shown to cause β-catenin nuclear translocation and AJ disassembly in transformed cells (32). Cortactin promotes actin polymerization and stabilizes peripheral F-actin fibers, thus enhancing endothelial barrier integrity (33, 34). An intact microtubule network is critical for maintenance of endothelial barrier integrity (35–37). α-Tubulin is a building block of microtubules. Acetylation of α-tubulin is characteristic of microtubule stabilization. CS extract (CSE) has been shown to cause microtubule depolymerization in human umbilical vein ECs (38). However, it is unknown whether CS alters acetylation status of proteins important in maintenance of endothelial barrier integrity.

Histone deacetylase (HDAC) 6 is ubiquitously expressed and predominantly located in the cytoplasm (39). Inhibition of HDAC6 has recently been proposed as a novel, promising, therapeutic option for a variety of disorders, including cilial dysfunction (40), cardiac dysfunction (41), Alzheimer's disease (42, 43), depression (44, 45), diabetes (46), and cancers (47). HDAC6 inhibitors also attenuate thrombin-induced EC permeability *in vitro* (48) and abrogate LPS-induced ALI in mice (49). HDAC6 knockout mice do not have a visible abnormal phenotype (50), but are also resistant to LPS-induced ALI (51). However, the role of HDAC6 in CSE-induced endothelial permeability and CS priming of ALI has not been studied. Overexpression of HDAC6 causes global deacetylation of α-tubulin (39), whereas HDAC6 knockout mice display hyperacetylated α-tubulin (50), suggesting that α-tubulin is a major target of HDAC6. HDAC6 also deacetylates cortactin (52, 53) and β-catenin (32). The objective of this study was to determine the role of HDAC6 in CS priming for ALI.

In this study, we demonstrate that CS increased HDAC6 phosphorylation *in vivo* and *in vitro*. Inhibition of HDAC6 blunted CSE-induced EC barrier dysfunction and CS priming for LPS-induced lung edema. Inhibition of HDACs also prevented ALI induced by infection of *Pseudomonas aeruginosa*. We further demonstrate a novel mechanism by which CS increased lung EC permeability and susceptibility to ALI, likely through oxidative stress–induced Akt inactivation and subsequent glycogen synthase kinase (GSK)-3β activation. Activated GSK-3β may phosphorylate HDAC6 (serine [Ser]-22), thus activating HDAC6, leading to α-tubulin deacetylation and microtubule disassembly. Inhibition of HDAC6 may be a novel therapeutic option for ALI, including CS priming of ALI.

Materials and Methods

Cells and Reagents

Primary bovine pulmonary artery ECs (PAECs) were purchased from Vec Technologies, Inc. (Rensselaer, NY) and propagated in Eagle's minimum essential medium containing 10% FBS and sodium pyruvate. Primary human lung microvascular ECs (LMVECs) were purchased from Lonza Inc. (Allendale, NJ) and propagated in microvascular endothelial growth medium-2 containing 5% FBS. All primary ECs were used between passages 2 and 7 in this study. LPS (*Escherichia coli* [055:B5]), thrombin, *Griffonia simplicifolia* lectin, N-acetyl cysteine (NAC), and antibodies directed against acetylated α-tubulin, phospho-HDAC6 (Ser22), and vinculin were from Sigma-Aldrich (St. Louis, MO). LPS was filtered with 0.2-μm filters. Taxol and trichostatin A (TSA) were purchased from Tocris (R&D Systems, Minneapolis, MN); Tubacin was from Enzo Life Sciences (Farmingdale, NY); HDAC6 small interfering RNA (siRNA), control siRNA, and antibodies directed against actin and VE-cadherin were from Santa Cruz Inc. (Santa Cruz, CA); antibodies directed against HDAC6, Akt, phospho-Akt (Ser473), phospho–GSK-3β (Ser9), and α-tubulin were from Cell Signaling Technologies (Danvers, MA); antibody directed against GSK-3β was from BD Biosciences (San Diego, CA); acetylated low-density lipoprotein (Ac-LDL) was from Life Technologies (Waltham, MA); and antibodies directed against von Willebrand factor (vWF) were from Dako (Carpinteria, CA). *P. aeruginosa* (strain: PA103) was a kind gift from Dr. Troy Stevens (University of South Alabama, Mobile, AL) (54).

CS Exposure of Mice

All animal protocols were approved by the Institutional Animal Care and Use Committee of the Providence Veterans Affairs Medical Center (Providence, RI) and comply with the Health Research Extension Act and the U.S. Public Health

Service Policy. Male C57BL/6 mice (6–8 weeks old) and AKR mice (6 weeks old) were continuously exposed to CS or room air (RA) for 6 hours per day using a TE-10 mouse smoking machine (Teague Enterprises, Woodland, CA) and 3R4F reference cigarettes (University of Kentucky, Tobacco Research Institute, Lexington, KY), as we previously described (25). The smoking chamber atmosphere was monitored for total suspended particles at a concentration of 120 mg/m^3 by burning three cigarettes at a time. The smoke was a mixture of sidestream (89%) and mainstream (11%) smoke.

Isolation of Mouse LMVECs

Male C57BL/6 mice (6 weeks old) were exposed to RA or CS for 6 hours. After overnight rest, cortical lung tissues from five mice in each group were collected, pooled, and enzymatically digested using a mouse lung dissociation kit (Miltenyi Biotec, San Diego, CA) and gentleMACs Dissociator (Miltenyi Biotec, San Diego, CA) protocols. Cell suspensions were passed through a 70-μm mesh. The cells were then incubated with mouse anti-CD45 microbeads (Miltenyi Biotec) for 15 minutes at 4°C. CD45$^+$ cells (leukocytes) were depleted using a MACS column and magnetic field (Miltenyi Biotec). The flowthrough from the column containing CD45$^-$ cells was collected, washed, and then incubated with mouse anti-CD31 microbeads (Miltenyi Biotec) for 15 minutes at 4°C. CD31$^+$ cells were enriched using a MACS column and magnetic field (Miltenyi Biotec). CD31$^+$ cells were then eluted from the column and resuspended in MCDB131 complete media (Vec Technologies). The freshly isolated cells, referred to as passage (P) 0, were counted (~20 × 10^6 cells/five mice) and plated onto a T75 flask coated with 0.2% gelatin and allowed to grow to 100% confluency (usually ~4–5 days). Culture media were changed every day for the first 3 days of culture and then every other day. Phase images were taken each day for recording purposes. The confluent P0 cells were replated (referred to as P1) onto both collagen-coated glass coverslips for characterization and electrical cell impedance sensor (ECIS; Applied Biophysics, Troy, NY) arrays for experiments.

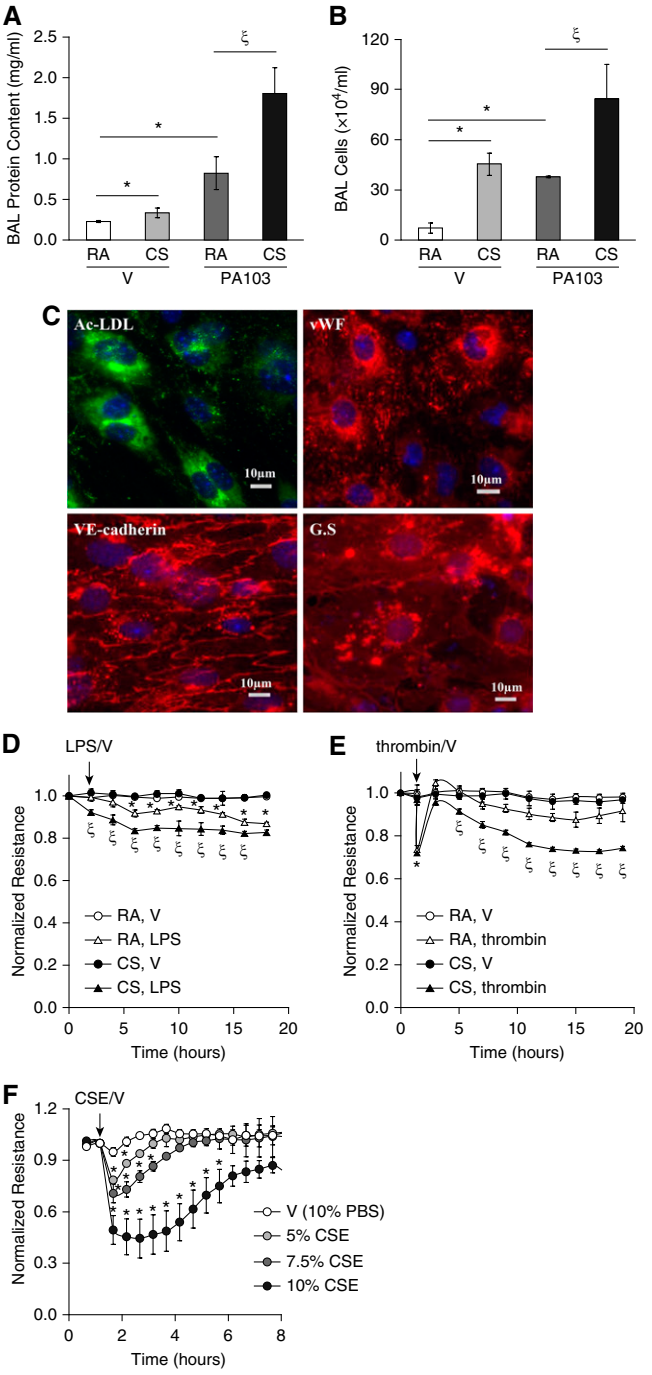

Figure 1. Cigarette smoke (CS) exacerbated acute lung injury (ALI) *in vivo* and increased lung microvascular endothelial cell (LMVEC) permeability *in vitro*. (*A* and *B*) Male C57BL/6 mice (6–8 weeks old) were exposed to room air (RA) or CS for 6 hours. After 1 hour of rest, mice were intratracheally administered 5 × 10^3 CFU of *Pseudomonas aeruginosa* (PA103) or equal volume of saline as vehicle (V). 24 hours later, mice were killed and bronchoalveolar lavage (BAL) protein levels and inflammatory cell counts were assessed. Four to six mice per group were used. The data are presented as the mean ± SE. ANOVA and Tukey-Kramer *post hoc* test was used to determine statistically significant difference across means among groups. *$P < 0.05$ versus (RA + V); $^{\xi}P < 0.05$ versus (RA + PA103); (*C–E*) 6-week-old male C57BL/6 mice were exposed to RA or CS for 6 hours. After overnight rest, LMVECs were isolated from cortical lung tissues, as described in Materials and Methods. A fraction of the isolated cells at passage (P) 1 were characterized by fluorescent microscopy (*C*) using EC markers, including acetylated low-density lipoprotein (Ac-LDL) uptake, von Willebrand factor (vWF), and vascular

Characterization of Isolated Mouse LMVECs

The 80–90% confluent P1 cells grown on coverslips were characterized using the EC markers, Ac-LDL uptake, vWF, and VE-cadherin, and through binding to the microvascular EC marker, *G. simplicifolia*. The cells were repeatedly characterized at each passage. To perform Ac-LDL uptake assay, isolated cultured cells were labeled with Alexa Fluor 488–conjugated Ac-LDL at 10 μg/ml in complete MCDB-131 media for 4 hours at 37°C. Cells were then washed and fixed with 4% paraformaldehyde. The nuclei were counterstained with 4′,6-diamidino-2-phenylindole staining. Images were visualized and acquired by fluorescence microscopy. For lectin staining, fixed cells were labeled with *G. simplicifolia*. For other staining, cells were fixed with 4% paraformaldehyde and then labeled with antibodies directed against vWF and VE-cadherin.

Intratracheal Administration of LPS and *P. aeruginosa*

P. aeruginosa (PA103) were grown on solid tryptic soy agar and resuspended in sterile PBS. The concentrations of PA103 were determined by a series of dilutions, cells replated on agar plates, and quantitated by CFUs. Mice were anesthetized with 3% isoflurane and intratracheally instilled with 2.5 mg/kg LPS (dissolved in saline), an equal volume of saline (control), or certain doses (i.e., 10^5 CFU) of PA103. At 4 hours (PA103) or 24 hours (LPS) after treatment, mice were killed, and ALI was assessed.

Preparation of CSE

As we described previously (25), mainstream smoke from Kentucky research cigarettes (3R4F) was drawn into 30 ml of PBS by a vacuum. Each cigarette was lit for 5 minutes, and five cigarettes were used per 30 ml of PBS. Control solution (sham PBS) was prepared using the same method, except that the cigarettes were unlit. The CSE–PBS was diluted with culture medium and used immediately.

Assessment of Protein Concentrations and Inflammatory Cell Counts in Bronchoalveolar Lavage Fluid

As we described previously (55), mice were killed using an overdose of pentobarbital (120 mg/kg) through intraperitoneal injection. The lung was lavaged with 600 μl of sterilized saline. The protein concentrations and the total numbers of inflammatory cells in the bronchoalveolar lavage (BAL) fluid were assessed by detergent-compatible protein assay and TC20 Automated Cell Counter (Bio-Rad, Hercules, CA), respectively.

Endothelial Monolayer Permeability Assay

Endothelial monolayer permeability assay was performed as we previously described (56) using the ECIS technique.

Transfection of siRNA

As we previously described (57), ECs were plated on ECIS arrays at 70% confluence. After 24 hours, cells were transfected with HDAC6 siRNA or scrambler siRNA as control using Lipofectamine 2,000 transfection reagent (Life Technologies/ ThermoFisher, Waltham, MA). After 72 hours, cells were treated with vehicle or CSE for varying times. Monolayer permeability was monitored and cells were collected for assessment of HDAC6 protein levels by the end of experiment.

Assessment of Microtubule Monomers and Polymers by Microtubule Extraction:

As previously described (58), ECs were rinsed with PBS and then lysed *in situ* with extraction buffer containing 1% vol/vol Triton-X 100 and protease and phosphatase inhibitors cocktail for 5 minutes at room temperature. The supernatant (free microtubule [MT] monomers) was collected and dissolved in Laemmli sample buffer. The remaining MT ghost (MT polymers) was dissolved *in situ* and collected by scraping the plates with Laemmli sample buffer. DNA in the MT ghost was severed by running samples through a 22-gauge needle 10 times. Both dissolved MT monomers and polymers were collected and equal volume loading of these supernatants (MT monomers) and MT ghost (polymers) was subjected to Western blot analysis.

Statistical Analysis

For animal studies, three to seven mice per group were used. All experiments using cultured cells were performed at least three independent times. Data are presented as mean (±SE). ANOVA and Tukey-Kramer *post hoc* test were used to determine statistically significant difference across means among three or more groups. Differences across means are considered significant when P was less than 0.05. Details on methods used for statistical analyses and significance are indicated in the figure legends.

Results

CS Exacerbated *Pseudomonas*-Induced ALI in Mice

We have previously shown that CS exacerbated LPS-induced ALI (25). The

Figure 1. (Continued). endothelial–cadherin, as well as LMVEC marker, *Griffonia simplicifolia* (GS) binding. The nuclei were counterstained with 4′,6-diamidino-2-phenylindole staining. *Scale bars*, 10 μm. Representative images from mice exposed to CS are shown. The remaining cells at P1 were plated onto electrical cell impedance sensor (ECIS) arrays at equal numbers of cells (2.5×10^5 cells/ well). After overnight attachment, cells were treated with vehicle (V), LPS (1 μg/ml), or thrombin (2 U/ml) for 20 hours and monolayer permeability was assessed by measuring electrical resistance across a monolayer using ECIS (*D* and *E*). Four independent experiments with duplicated ECIS wells for each condition each time were conducted. (*F*) Primary human LMVECs were treated with vehicle (V, 10% PBS) or varying concentrations of cigarette smoke extract (CSE) for indicated times, and monolayer permeability was assessed by ECIS. Three independent experiments with duplicated ECIS wells for each condition each time were conducted. For *D–F*, the data are presented as the mean ± SE of the normalized electrical resistance at the selected time points relative to their initial resistance. ANOVA and Tukey-Kramer *post hoc* test was used to determine statistically significant difference across means among groups. $^*P < 0.05$ versus (RA + V) (*D* and *E*) or V (*F*); $^{\xi}P < 0.05$ versus (RA + LPS) (*D*) or (RA + thrombin) (*E*). *Arrows* indicate the time for addition of treatments.

common human infections, such as pneumonias, are often caused by *P. aeruginosa*, a gram-negative aerobic bacterium. *P. aeruginosa* infections are difficult to eradicate, and often develop resistance to antibiotics, therefore contributing to the most serious fatal infections and ALI, particularly in those patients immunosuppressed by severe trauma, burns, and wounds. Similar to other gram-negative bacteria, *P. aeruginosa* uses LPS to maintain outer membrane structural integrity and to serve as the key endotoxin and mediator of host–pathogen interactions. Therefore, it is clinically important to test if CS increases the susceptibility to *P. aeruginosa*–induced ALI. We found that CS pre-exposure exacerbated *P. aeruginosa* (PA103)–induced lung edema, as indicated by significant increases in BAL protein content (Figure 1A) and BAL inflammatory cell counts (Figure 1B). These data further support the concept that CS primes individuals for ALI.

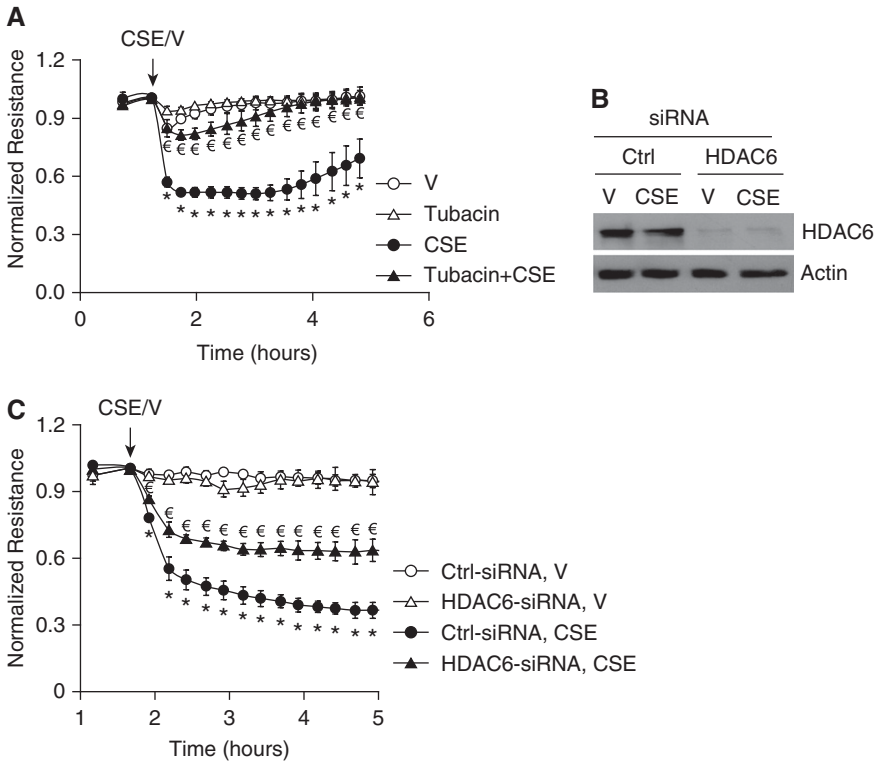

Figure 2. Blocking histone deacetylase (HDAC) 6 blunted CSE-induced EC barrier dysfunction *in vitro*. (*A*) Bovine pulmonary artery ECs (PAECs) were preincubated with 100 nM tubacin for 1 hour and then treated with vehicle (V; 15% PBS) or 15% CSE in the absence or presence of 100 nM tubacin for indicated times. Monolayer permeability was assessed by ECIS. (*B* and *C*) Human LMVECs were transfected with control siRNA (Ctrl-siRNA) or HDAC6 siRNA (HDAC6-small interfering RNA [siRNA]). At 72 hours after transfection, cells were exposed to vehicle (V; 15% PBS) or 15% CSE for up to 5 hours and monolayer permeability was assessed by ECIS (*C*). Cells were collected from arrays after ECIS for assessment of HDAC6 protein levels by Western blot (*B*). Three independent experiments with duplicated ECIS wells for each condition each time were conducted. (*B*) Representative immunoblots. For *A* and *C*, the data are presented as the mean ± SE of the normalized electrical resistance at the indicated time points relative to their initial resistance. ANOVA and Tukey-Kramer *post hoc* test was used to determine statistically significant difference across means among groups. $^{*}P < 0.05$ versus V (*A*) or (Ctrl-siRNA + V) (*C*); $^{€}P < 0.05$ versus CSE (*A*) or (Ctrl-siRNA + CSE) (*C*). *Arrows* indicate the time for addition of treatments.

CS Promoted LMVEC Permeability *In Vitro*

Epidemiologic evidence (6, 8, 9) and our previous animal studies (25) have revealed that CS increases susceptibility to the development of ALI. To begin to understand the contribution of lung ECs to CS-induced increased susceptibility to ALI, we examined the effect of CS exposure on lung endothelial barrier function *in vitro*. LMVECs were isolated from mice exposed to CS or RA for 6 hours and rested overnight. The isolated cells at P1 were characterized by the EC markers, including Ac-LDL uptake, vWF, and VE-cadherin, as well as the LMVEC marker, binding to *G. simplicifolia* lectin (Figure 1C). The isolated cells at P1 were also subjected to treatments of LPS, thrombin, or vehicle controls. A low dose of LPS increased endothelial monolayer permeability in LMVECs isolated from mice exposed to RA. However, LMVECs isolated from mice exposed to CS showed a much greater permeability after LPS challenge (Figure 1D). Thrombin rapidly increased monolayer permeability, and the barrier function was almost recovered over time in LMVECs isolated from mice exposed to RA (Figure 1E). The peak increase in permeability of cells isolated from CS-exposed mice was not different from cells isolated from RA-exposed mice. However, after a brief recovery, the endothelial barrier of cells from CS-exposed mice underwent a second gradual, sustained increase in permeability, which did not recover over 20 hours (Figure 1E). These results indicate that CS pre-exposure had an injurious impact on lung endothelial barrier function.

We have previously shown that CSE increases PAEC permeability (25). In this study, we also assessed the effect of CSE on barrier integrity of human LMVECs *in vitro*. Not surprisingly, CSE dose-dependently increased monolayer permeability of primary cultures of human LMVECs, and barrier function was slowly recovered over time (Figure 1F).

Inhibition of HDAC6 Blunted CSE-Induced EC Barrier Dysfunction *In Vitro* and Attenuated CS-Induced Priming for ALI *In Vivo*

Endothelial barrier function is maintained by intercellular AJs, cortactin-associated cortical F-actin, and intact microtubules. AJs (32), cortactin (52, 53), and microtubules (39) are potential targets of HDAC6 deacetylation. To determine the role of HDAC6 in CS-induced increased endothelial permeability, HDAC6 was inhibited by a specific pharmacological inhibitor, tubacin (59). The IC_{50} (concentration of an inhibitor where the

response is reduced by half) of tubacin inhibiting HDAC6 was reported to be 2.5 μM in cultured cells (59). We tested the effects of varying concentrations of tubacin (i.e., 10 nM, 50 nM, 100 nM, 1 μM, and 10 μM) on CSE-induced endothelial permeability and found that 50 nM–1 μM of tubacin blunted CSE-induced increase in endothelial permeability, with 100 nM being the optimal concentration. Neither the lower (10 nM) nor the higher (10 μM) doses of tubacin were effective (data not shown). Tubacin (100 nM) treatment alone had no significant effect on endothelial permeability, but almost completely protected against CSE-induced increase in monolayer permeability (Figure 2A). HDAC6 siRNA was also used to suppress HDAC6 protein expression (Figure 2C). Suppression of HDAC6 expression by siRNA also attenuated CSE-induced increased permeability in human LMVECs (Figure 2C). These results suggest that HDAC6 activation contributes to CSE-induced increase in human LMVEC permeability.

To determine the role of HDAC6 activation in CS priming for the development of ALI, we tested the effects of HDAC6 inhibitors, TSA and tubacin, on CS priming for ALI after LPS challenge. Neither TSA nor tubacin alone had any effect on BAL protein levels or inflammatory cell counts (Figures 3A and 3B). Similar to our previous results (25), 6-hour CS pre-exposure exacerbated LPS-induced elevation in BAL protein content; the effect was significantly blunted by inhibition of HDAC6 with either TSA or tubacin (Figure 3A). TSA and tubacin also prevented CS plus LPS–induced lung inflammation, as assessed by

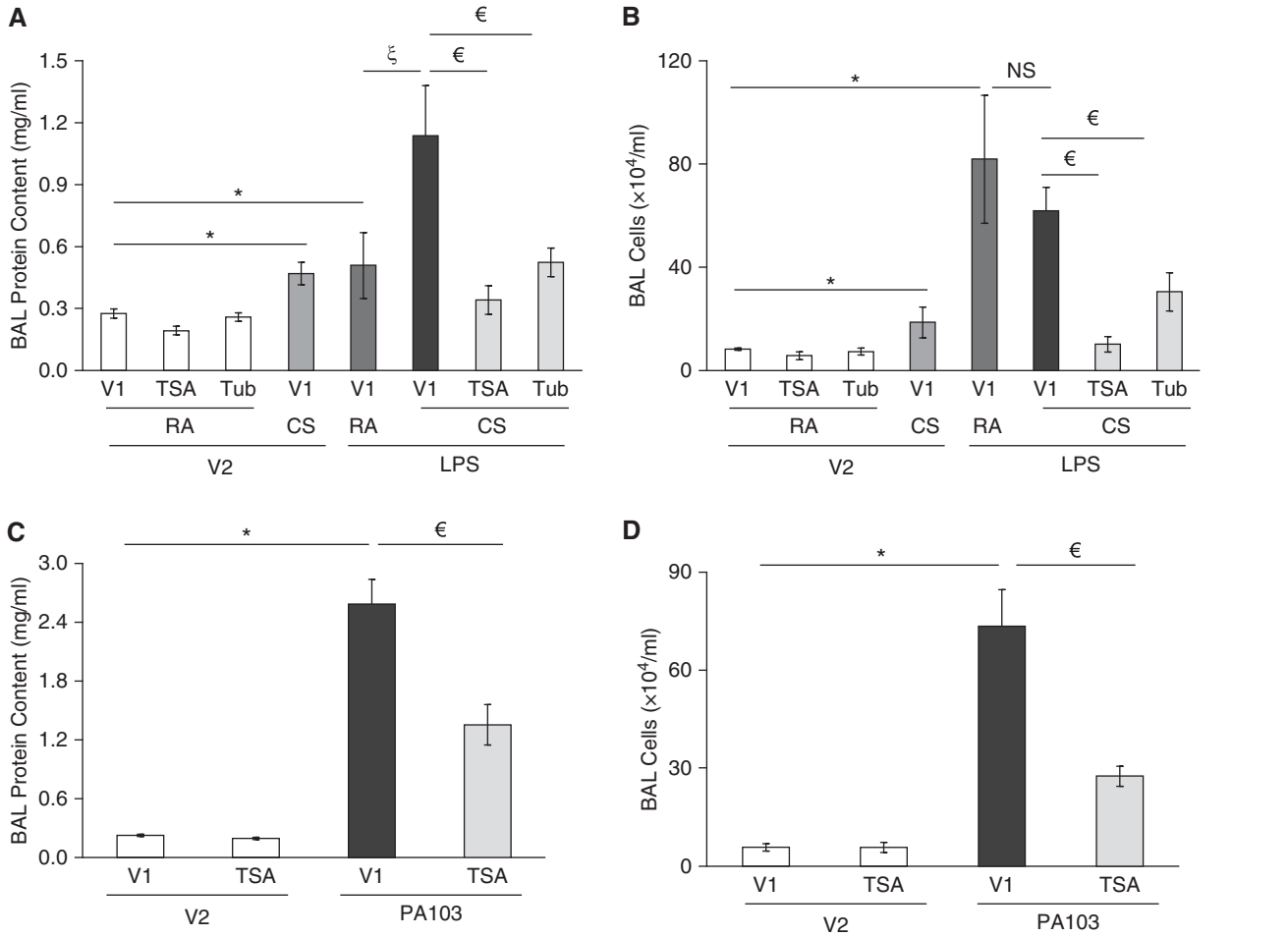

Figure 3. Blocking HDAC6 attenuated CS priming for LPS-induced ALI and *P. aeruginosa*–induced ALI in mice. (*A* and *B*) Male C57BL/6 mice (6–8 weeks old) were intraperitoneally administered the HDAC6 inhibitors trichostatin A (TSA; 20 mg/kg) or tubacin (Tub; 20 mg/kg) or vehicle (V1). After 30 minutes, mice were exposed to RA or CS for 6 hours. After 1 hour of rest, mice were given 2.5 mg/kg LPS or saline (vehicle, V2) intratracheally. After 24 hours, BAL protein levels (*A*) and total numbers of inflammatory cells in BAL fluid (*B*) were assessed. Three to seven mice per group were used. (*C* and *D*) Male C57BL/6 mice (6–8 weeks old) were intraperitoneally administered TSA (20 mg/kg) or vehicle (V1). After 30 minutes, mice were intratracheally administered 1×10^5 CFU of *P. aeruginosa* or an equal volume of saline (vehicle, V2). After 4 hours, mice were killed and BAL protein levels and inflammatory cell counts were assessed. Four to six mice per group were used. The data are presented as the mean ± SE. ANOVA and Tukey-Kramer *post hoc* test was used to determine statistically significant difference across means among groups. $^*P < 0.05$ versus (RA + V1 + V2) (*A* and *B*) or (V1 + V2) (*C* and *D*); $^{\zeta}P < 0.05$ versus (RA + V1 + LPS) (*A*); $^{€}P < 0.05$ versus (CS + V1 + LPS) (*A* and *B*) or (V1 + PA103) (*C* and *D*). NS, not significant.

BAL inflammatory cell counts (Figure 3B).

Inhibition of HDACs also Blunted *P. aeruginosa*–Induced ALI

To determine if inhibition of HDACs blunts lung edema caused by other agents, we tested the effect of TSA on lung edema induced by *P. aeruginosa*, a potentially fatal cause of lung infection and ALI in humans. We found that inhibition of HDACs by TSA indeed blunted *P. aeruginosa* (PA103)–induced lung edema, as indicated by significant attenuation of increases in BAL protein content (Figure 3C) and BAL inflammatory cell counts (Figure 3D).

CS Increased HDAC6 Phosphorylation *In Vitro* and *In Vivo*

To elucidate the mechanism of CS-induced HDAC6 activation, we examined post-translational modifications of HDAC6. Although HDAC6 total protein levels were not significantly altered in cultured PAECs exposed to CSE for up to 6 hours (Figures 4A and 4C), PAECs exposed to CSE for varying time periods demonstrated a time-dependent increase in HDAC6 phosphorylation at Ser-22 (Figures 4A and 4B). We also noted that CSE exposure induced a protein with a higher molecular weight and recognized by HDAC6 antibody, in a time-dependent manner (Figure 4A), suggesting an additional unknown post-translational modification of HDAC6 *in vitro*. A similar increase in HDAC6 phosphorylation of Ser-22 was also shown in lung homogenates of mice exposed to CS for 3 weeks (Figures 4D and 4E). Unlike cultured PAECs, HDAC6 total protein levels were reduced in lung homogenates of mice exposed to CS for 3 weeks (Figures 4D and 4F).

CSE Inactivated Akt and Activated GSK-3β *In Vitro*

Akt is activated by phosphorylation at threonine-308 and Ser-473 (60). Activated Akt phosphorylates GSK-3β at Ser-9, thus inhibiting its kinase activity (60). GSK-3β is a potential kinase for phosphorylation of HDAC6 at Ser-22 (61). Therefore, we assessed the effects of CS on Akt/GSK-3β signaling. PAECs exposed to CSE for varying times (30 minutes to 6 hours) demonstrated a time-dependent reduction in Akt phosphorylation at Ser-473 (Figures 5A and 5B), indicating inactivation of Akt. In line with the decrease in Akt phosphorylation, exposure of PAECs to CSE for 30 minutes to 3 hours also significantly reduced GSK-3β phosphorylation at Ser-9 (Figures 5D and 5E), indicating activation of GSK-3β. Decreased phosphorylation of Akt–Ser-473 and GSK-3β–Ser-9 were also observed in lung tissue of mice exposed to CS for 6 hours (Figures 5G–5I). Although CSE did not significantly alter protein levels of either Akt or GSK-3β in cultured PAECs (Figures 5A, 5C, 5D, and 5F), the total protein levels of both Akt and GSK-3β were significantly diminished in lung homogenates of mice exposed to CS for 6 hours (Figures 5G–5I). The ratio of either phosphorylated Akt to total Akt (Figure 5H) or phosphorylated GSK-3β to total GSK-3β (Figure 5I) was not altered in lung homogenates of mice exposed to CS for 6 hours. These results suggest that it is likely that the decrease in the levels of

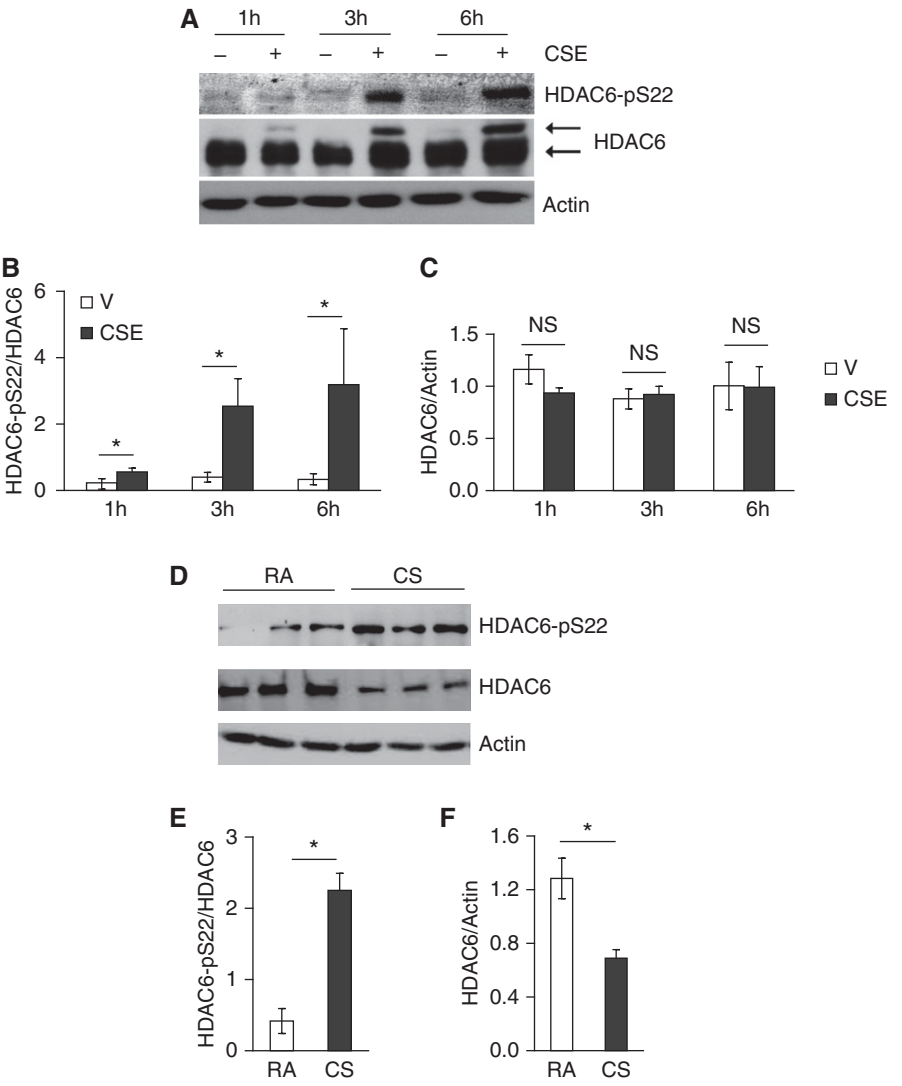

Figure 4. CS promoted HDAC6 phosphorylation *in vitro* and *in vivo*. Bovine PAECs were treated with vehicle (10% PBS) or 10% CSE for the indicated times (*A–C*); 6-week-old male AKR mice were exposed to RA or CS for 3 weeks at 4 days per week, as described in Materials and Methods (*D–F*). The levels of HDAC6 total protein and phosphorylated HDAC6 at Ser-22 in cell lysates and lung homogenates were assessed. Actin was used as protein loading controls. (*A* and *D*) Representative images. Densitometry was performed on immunoblots; $n = 3$ for *A–C* and $n = 4$ for *D–F*. The data are presented as the mean ± SE of the ratio of the densitometry of phospho-HDAC6 (Ser-22) to total HDAC6 (*B* and *E*) and of total HDAC6 to actin (*C* and *F*). ANOVA and Tukey-Kramer *post hoc* test was used to determine statistically significant difference across means among groups. $^*P < 0.05$ versus respective V (*B*) or RA (*E* and *F*).

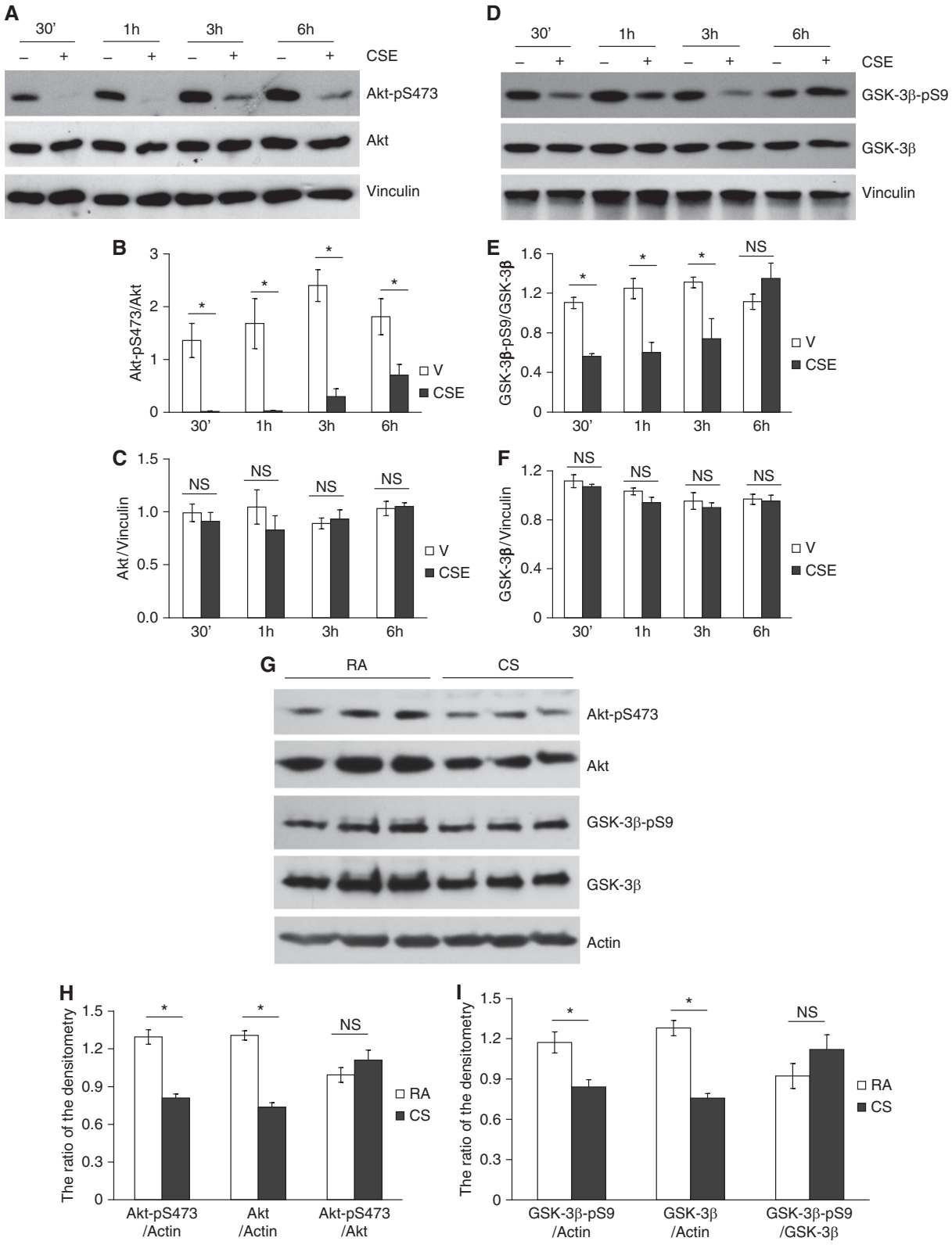

Figure 5. CSE inactivated Akt and activated glycogen synthase kinase (GSK)-3β *in vitro* and *in vivo*. Bovine PAECs were treated with vehicle (V; 10% PBS) or 10% CSE for the indicated times (*A–F*); 6- to 8-week-old male C57BL/6 mice were exposed to RA or CS for 6 hours, as described in Materials and Methods (*G–I*). Akt/GSK-3β total protein levels and Akt phosphorylation at Ser-473 and GSK-3β phosphorylation at Ser-9 in cell lysates and lung homogenates were assessed. Vinculin and actin were used for protein loading controls. Three independent experiments. Densitometry was performed on

phosphorylated Akt and GSK-3β in lung tissues was due to the decrease in total Akt and GSK-3β protein levels.

CSE Caused GSK-3β Activation and Subsequent HDAC6 Phosphorylation, Likely through Oxidative Stress–Mediated Akt Inhibition

We have previously shown that CS increases reactive oxygen species (ROS) levels in lung tissues and cultured lung ECs, and that the antioxidant, NAC, prevented CSE-induced endothelial monolayer permeability (25). In this study, we found that NAC also prevented CSE-induced decrease in Akt phosphorylation and GSK-3β phosphorylation and increase in HDAC6 phosphorylation in PAECs (Figures 6A and 6B). Our results suggest that CS activates HDAC6, likely via oxidative stress–induced Akt inactivation and subsequent GSK-3β activation.

CSE Caused Lung Endothelial Barrier Dysfunction via α-Tubulin Deacetylation and Subsequent Microtubule Disassembly

Because α-tubulin is a major substrate of HDAC6 (39, 50), we assessed the effect of CSE on α-tubulin acetylation and found that CSE dramatically reduced α-tubulin acetylation (Figures 7A–7C). An intact microtubule network is essential to endothelial barrier integrity (30). Correlating with loss of endothelial barrier integrity, CSE also caused microtubule depolymerization, as indicated by increased monomers and decreased polymers of α-tubulin in ECs exposed to CSE for varying times (Figures 7D and 7E). The microtubule stabilizer, taxol, enhanced α-tubulin acetylation (data not shown) and also abolished CSE-induced increase in endothelial permeability (Figure 7F). These results suggest that CSE increases EC permeability, likely via α-tubulin deacetylation and subsequent microtubule disassembly.

Discussion

Growing epidemiological evidence has demonstrated that both active and passive CS exposure increases susceptibility to the development of ALI (6, 8, 9). The mechanism underlying CS priming for ALI is not well understood. Donor lungs from smokers are heavier and have worse clinical outcomes after transplantation, suggesting that smokers' lungs are edematous (62). This notion is supported by our animal studies, demonstrating that brief CS exposure increases lung wet:dry weight ratio and exacerbates LPS- (25) and *Pseudomonas*-induced lung edema in mice. Inhalation of CS *in vivo* has complex effects on multiple cell types. Lung edema may be caused by increased alveolar endothelial and epithelial permeability and/or impaired alveolar fluid clearance. Greater alveolar epithelial permeability has been reported in human smokers (15) and guinea pigs exposed to CS (14, 16). CS exposure also affects pulmonary ECs. For example, CS causes pulmonary endothelial dysfunction in otherwise healthy young smokers (18) and guinea pigs (19, 20). Pulmonary endothelial denudation has also been documented in chronic smokers with COPD (23). We (25) and others (14, 27) have previously shown that CS exposure increases lung vascular permeability in animal models. In addition, CSE increases monolayer permeability of cultured lung ECs (24–26). Although the CSE exposure of cultured cells is a widely used and acceptable *in vitro* system to model CS effects on endothelium and epithelium (13, 63), the nature and concentrations of CS components may differ between CS inhalation *in vivo* and CSE exposure *in vitro*. It was unknown if CS indeed increased LMVEC permeability *in vivo*, due to the limitations of *in vivo* and *in vitro* models. In this study, we used LMVECs isolated from CS-exposed mice to determine the consistency and discrepancy of CS effects on lung ECs using an *in vivo* mouse model, a freshly isolated LMVECs, and a primary LMVECs exposed to CSE *in vitro* model. We provide direct evidence that LMVECs isolated from mice exposed to CS were more susceptible to increased permeability after a second insult, LPS, or thrombin. This result is consistent with our previous *in vivo* and *in vitro* findings (25). Our data indicate that diminished lung EC barrier integrity contributes to increased susceptibility to ALI.

Inhibition of HDACs by TSA and butyrate has been shown to prolong survival and attenuate ALI induced by LPS (49), cecal ligation and puncture–induced polymicrobial sepsis (64), and mechanical ventilation (65). HDAC6 knockout mice were also resistant to LPS-induced ALI (51). In this study, we show that inhibition of HDACs by TSA significantly blunted lung edema and lung inflammation induced by infection of *P. aeruginosa*, a clinically relevant model of pneumonia and ALI. It has been suggested that HDAC6 inhibitors protect against ALI by suppressing inflammation (66). CS causes lung inflammation (11–13). A novel finding of this study is that inhibition of HDAC6 by a specific inhibitor, tubacin, significantly protected against CS priming of LPS-induced ALI. We further demonstrated that both pharmacological and molecular inhibition of HDAC6 blunted CSE-induced barrier dysfunction of human LMVECs *in vitro*. Our data suggest that the direct effect of HDAC6 inhibition on lung endothelial barrier integrity contributes to its protection against CS priming for ALI. Our results further support the notion that inhibition of HDAC6 is a novel therapeutic option for ALI by maintaining endothelial barrier integrity and by attenuating lung inflammation.

Nuclear HDACs, such as HDAC2, are decreased in lung tissues of smokers (67). Diminished nuclear HDAC expression has been implicated in pathogenesis of COPD via epigenetic histone modifications and subsequent NF-κB–mediated lung inflammation (11–13). In contrast to nuclear HDACs, cytoplasmic HDAC6 expression is elevated in lung tissues of chronic smokers with COPD (40). In our experimental model, HDAC6 protein levels were not changed in cultured lung ECs exposed to CSE *in vitro*, but significantly decreased in lung tissues of mice exposed to CS for 3 weeks. Further studies are necessary to determine HDAC6 expression in cell type–specific and exposure

Figure 5. (Continued). immunoblots of *A*, *D*, and *G*. The data are presented as the mean ± SE of the ratios of the densitometry of: phospho-Akt (Ser-473) to total Akt; phospho–GSK-3β (Ser-9) to total GSK-3β; total Akt to vinculin or actin; total GSK-3β to vinculin or actin; phospho-Akt (Ser-473) to actin; and phospho–GSK-3β (Ser-9) to actin; $n = 3$ for all panels. ANOVA and Tukey-Kramer *post hoc* test was used to determine statistically significant difference across means among groups. $^*P < 0.05$ versus respective V (*B* and *E*) or RA (*H* and *I*).

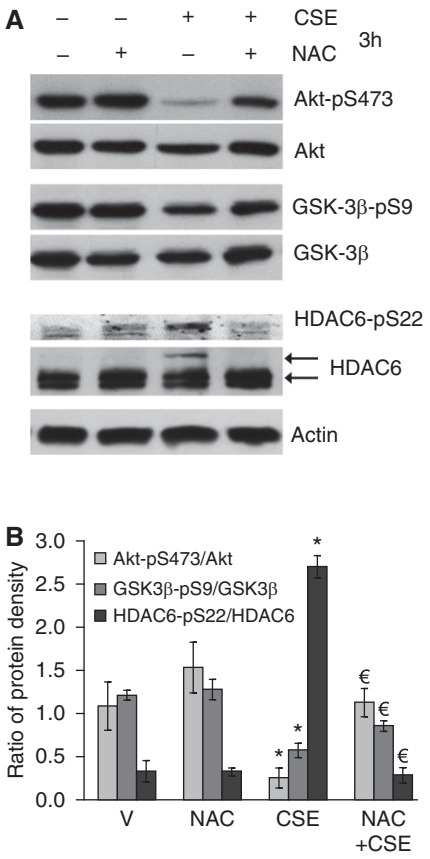

Figure 6. CSE caused GSK-3β activation and HDAC6 phosphorylation likely through oxidative stress–mediated Akt inactivation. Bovine PAECs were pretreated with 100 μM N-acetyl cysteine (NAC) for 30 minutes and then treated with vehicle or 10% CSE in the absence or presence of 100 μM NAC for 3 hours. Akt/GSK-3β/HDAC6 total protein levels, Akt phosphorylation at Ser-473, GSK-3β phosphorylation at Ser-9, and HDAC6 phosphorylation at Ser-22 in cell lysates were assessed. Actin was used as protein loading controls. (*A*) Three independent experiments. Densitometry was performed on immunoblots. The data are presented as the mean ± SE of the ratio of the densitometry of: phospho-Akt (Ser-473) to total Akt; phospho–GSK-3β (Ser-9) to total GSK-3β; and phospho-HDAC6 (Ser-22) to total HDAC6 (*B*); $n = 3$. ANOVA and Tukey-Kramer *post hoc* test was used to determine statistically significant difference across means among groups. $^{*}P < 0.05$ versus respective V; $^{€}P < 0.05$ versus CSE.

duration–dependent manners. Although there is a discrepancy regarding CS impacts on HDAC6 protein levels *in vivo* and *in vitro*, HDAC6 phosphorylation at Ser-22 was significantly elevated in lung tissues of mice exposed to CS for 3 weeks and in lung ECs exposed to CSE. HDAC6 activity is modulated by Tyr and Ser phosphorylation (68–70). Phosphorylation of HDAC6 at Ser-458, a residue found exclusively in higher primates (70), activates HDAC6 and increases autophagy (70). The G protein–coupled receptor kinase 2 phosphorylates HDAC6 at an unknown residue and activates HDAC6, thus promoting cell spreading and migration (68). In contrast, epidermal growth factor receptor–mediated phosphorylation of HDAC6 at Tyr-570 reduces HDAC6 deacetylase activity (71). In this study, enhanced HDAC6 phosphorylation at Ser-22 was associated with increased endothelial permeability and susceptibility to ALI. Moreover, inhibition of HDAC6 protected against CSE-induced EC barrier dysfunction *in vitro* and CS priming of LPS-induced and *P. aeruginosa*–induced lung edema *in vivo*. Our data suggest that HDAC6 phosphorylation at Ser-22 may activate HDAC6.

GSK-3β has been shown to phosphorylate HDAC6 at Ser-22 (61). Akt inhibits GSK-3β via phosphorylation of GSK-3β at Ser-9 (60). Akt is activated by phosphorylation at Ser-473 and threonine-308 (60). In this study, we show that Akt phosphorylation at Ser-473 and GSK-3β phosphorylation at Ser-9 were decreased, whereas HDAC6 phosphorylation at Ser-22 was increased, in cultured lung ECs exposed to CSE *in vitro* and in lung tissue of mice exposed to CS *in vivo*. Our data suggest that CS causes phosphorylation of HDAC6 at Ser-22, thus activating HDAC6 via Akt inhibition and subsequent GSK-3β activation.

Akt has two cysteine (Cys) residues, Cys-297 and Cys-311, in its activation loop; these are potential oxidation sites (72). ROS, components of CS and generated upon CS exposure, are increased in the blood of smokers (73). We have previously shown that CS increases ROS levels in lung tissues and cultured lung ECs, and that the antioxidant, NAC, prevented CS-induced lung vascular endothelial permeability *in vivo* and *in vitro* (25). In this study, we found that CSE-induced Akt inactivation, GSK-3β activation, and HDAC6 phosphorylation were prevented by NAC. It has been suggested that Akt oxidation may increase protein phosphatase (PP) 2A binding, thus increasing Akt dephosphorylation/inactivation (74). CSE has been shown to cause Akt degradation in lung fibroblasts (75). Because CSE dramatically reduced Akt phosphorylation without alteration of Akt total protein levels in cultured lung ECs, it is likely that increased dephosphorylation may be the major mechanism of Akt inactivation upon CS exposure in lung ECs. It is unknown whether CSE exposure causes Akt oxidation, leading to dephosphorylation/inactivation. In this study, although Akt total protein levels were not significantly altered in ECs exposed to CSE, they were significantly diminished in lung tissues of mice exposed to CS for 6 hours. Because the ratio of the phosphorylated Akt to total Akt protein was not altered in lung tissues, it is likely that the decrease in the levels of phosphorylated Akt in lung tissues was due to a decrease in Akt total protein as a result of protein degradation. It is unknown whether CS causes Akt oxidation, leading to Akt degradation *in vivo*. Because Akt total protein levels were not altered by CSE in cultured lung ECs, it is possible that the observed changes in Akt total protein *in vivo* are attributed to other cells than ECs. The discrepancy in CS effects on Akt/GSK-3β total protein levels *in vivo* and in *vitro* may also be due to differences in nature and concentrations of smoke inhalation *in vivo* and CSE exposure *in vitro*. Further studies are necessary to determine whether CS causes Akt oxidation, the site(s) of oxidation, and the roles of protein dephosphorylation and protein degradation in CS-induced Akt inhibition *in vitro* and *in vivo*. Taken together, our data suggest that CS may activate HDAC6 via Akt inhibition–dependent HDAC6 phosphorylation at Ser-22.

We noted that there is an additional modification in HDAC6. Identification of the nature of that modification will be pursued in future studies. β-Catenin (32) and cortactin (52, 53) are among the substrates of HDAC6 deacetylation. However, CSE did not significantly alter β-catenin acetylation (data not shown). Whether CS changes acetylation status of cortactin remains to be determined in future studies.

Microtubule stability is critical for maintenance of EC barrier integrity (35–37). For example, chemical disruption of microtubules increases EC permeability (37), whereas microtubule stabilization by taxol attenuates endotoxin-induced vascular leakiness and inflammation (36). Microtubule disassembly also contributes to thrombin-induced endothelial hyperpermeability

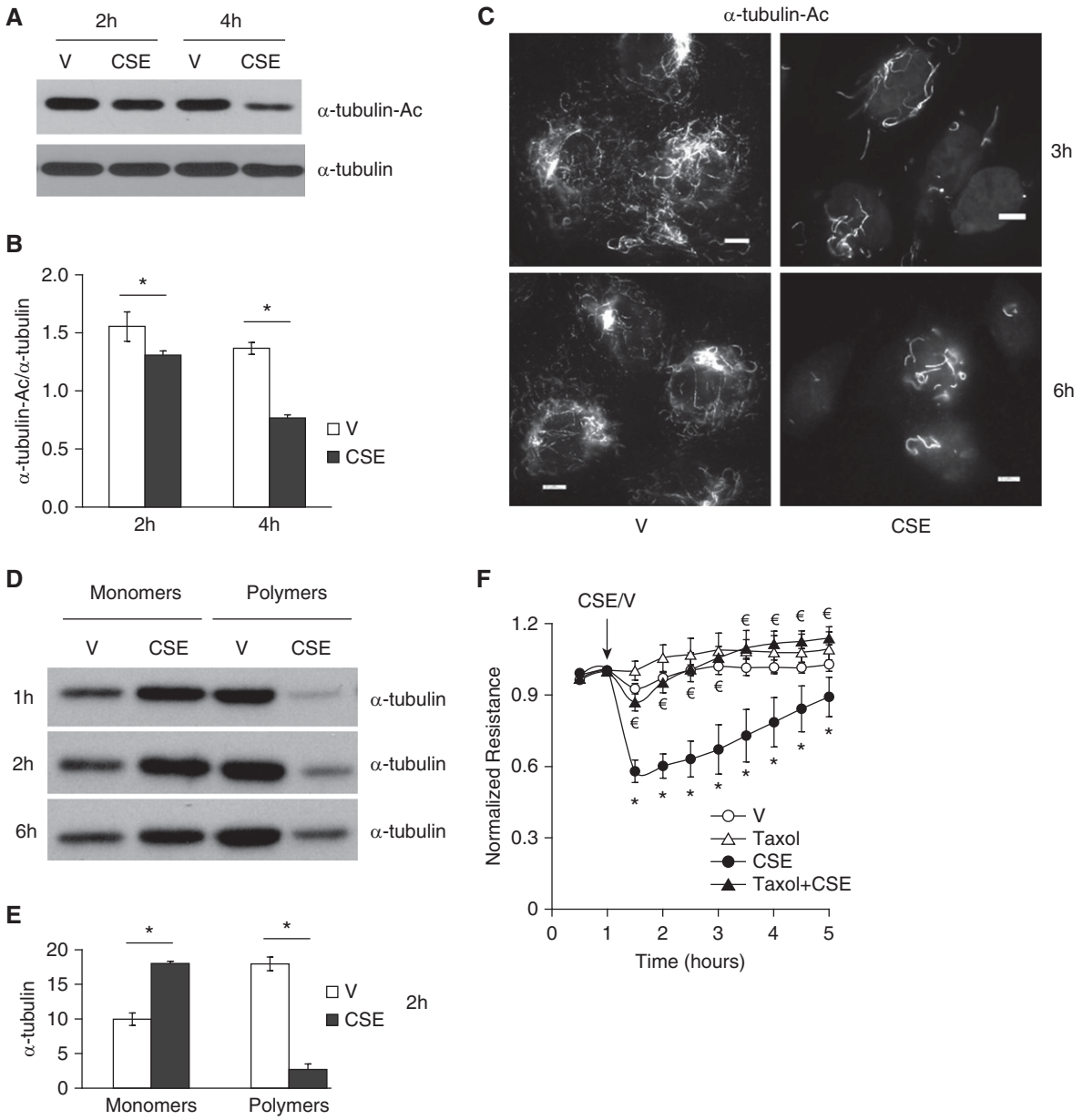

Figure 7. CSE caused lung endothelial barrier dysfunction, α-tubulin deacetylation, and microtubule disassembly. (*A–C*) Bovine PAECs were treated with vehicle (V; 10% PBS) or 10% CSE for the indicated times. Acetylated α-tubulin (α-tubulin-Ac) was assessed by Western blot (*A* and *B*) and immunofluorescence microscopy (*C*), using anti–acetylated α-tubulin antibody. α-Tubulin was also assessed. (*D* and *E*) Bovine PAECs were treated with vehicle (V; 10% PBS) or 10% CSE for the indicated times. Microtubule depolymerization was assessed by examining the levels of monomers and polymers of α-tubulin using microtubule extraction assay. (*F*) Bovine PAECs were pretreated with 5 μM Taxol for 30 minutes and then treated with vehicle (V; 10% PBS) or 10% CSE in the absence or presence of 5 μM taxol for the indicated times, and monolayer permeability was assessed. *Arrows* indicate the time of addition of treatments. (*A*, *C*, and *D*) Three independent experiments. Densitometry was performed on immunoblots for *A* and *D*. The data are presented as the mean ± SE of the ratio of the densitometry of α-tubulin-Ac to total α-tubulin (*B*), or as the mean ± SE of the densitometry of α-tubulin at 2 hours (*E*). ANOVA and Tukey-Kramer *post hoc* test was used to determine statistically significant difference across means among groups. $^{*}P < 0.05$ versus respective V; for *F*, the data are presented as the mean ± SE of the normalized electrical resistance at each time point relative to initial resistance; $n = 4$. ANOVA and Tukey-Kramer *post hoc* test was used to determine statistically significant difference across means among groups. $^{*}P < 0.05$ versus V; $^{€}P < 0.05$ versus CSE. *Scale bars*, 10 μm.

(35). Deacetylation of α-tubulin causes microtubule destabilization *in vivo* (76, 77). α-Tubulin is a major target of HDAC6 deacetylation (50). In a previous study, CSE was found to cause microtubule depolymerization via oxidative stress in human umbilical vein ECs (38). However, that study did not document the role of α-tubulin acetylation in CSE-induced barrier dysfunction. In this study, we found that CSE decreased α-tubulin acetylation and increased microtubule depolymerization in lung ECs. Similar to HDAC6 inhibition, increasing α-tubulin acetylation by the microtubule

stabilizer, taxol, attenuated CSE-induced EC barrier dysfunction. Our data suggest that CSE increases lung EC permeability via α-tubulin deacetylation and resultant microtubule depolymerization.

In summary, we have demonstrated that CS caused Akt inactivation, GSK-3β activation, and HDAC6 phosphorylation *in vivo* and *in vitro*. CS also caused α-tubulin deacetylation and microtubule disassembly. Inhibition of HDAC6 blunted CSE-induced EC barrier dysfunction *in vitro* and CS priming for LPS- and *Pseudomonas*-induced lung edema *in vivo*. Our data suggest that CS increases lung EC permeability, likely through Akt inhibition–induced HDAC6 activation and subsequent α-tubulin deacetylation and resultant microtubule depolymerization, as depicted in Figure E1 in the online supplement. Inhibition of HDAC6 may be a novel therapeutic option for ALI. ■

Author disclosures are available with the text of this article at www.atsjournals.org.

Acknowledgments: The authors acknowledge P20GM103652 (Harrington, Core B, Brown University, Providence, RI) for isolation and characterization of mouse lung microvascular endothelial cells. They also acknowledge Dr. Sarah Sayner (Department of Cell Biology and Neuroscience, University of South Alabama) for sharing the assessment protocol of microtubule monomers and polymers by microtubule extraction assay.

References

1. U.S. Department of Health and Human Services. The health consequences of smoking—50 years of progress: a report of the Surgeon General. Atlanta, GA: U.S. Department of Health and Human Services, Centers for Disease Control and Prevention, National Center for Chronic Disease Prevention and Health Promotion, Office on Smoking and Health; 2014.
2. Kang MJ, Lee CG, Lee JY, Dela Cruz CS, Chen ZJ, Enelow R, Elias JA. Cigarette smoke selectively enhances viral PAMP- and virus-induced pulmonary innate immune and remodeling responses in mice. *J Clin Invest* 2008;118:2771–2784.
3. Drannik AG, Pouladi MA, Robbins CS, Goncharova SI, Kianpour S, Stämpfli MR. Impact of cigarette smoke on clearance and inflammation after *Pseudomonas aeruginosa* infection. *Am J Respir Crit Care Med* 2004;170:1164–1171.
4. Feldman C, Anderson R. Cigarette smoking and mechanisms of susceptibility to infections of the respiratory tract and other organ systems. *J Infect* 2013;67:169–184.
5. Lugade AA, Bogner PN, Thatcher TH, Sime PJ, Phipps RP, Thanavala Y. Cigarette smoke exposure exacerbates lung inflammation and compromises immunity to bacterial infection. *J Immunol* 2014;192: 5226–5235.
6. Calfee CS, Matthay MA, Eisner MD, Benowitz N, Call M, Pittet JF, Cohen MJ. Active and passive cigarette smoking and acute lung injury after severe blunt trauma. *Am J Respir Crit Care Med* 2011;183:1660–1665.
7. Calfee CS, Matthay MA, Kangelaris KN, Siew ED, Janz DR, Bernard GR, May AK, Jacob P, Havel C, Benowitz NL, *et al*. Cigarette smoke exposure and the acute respiratory distress syndrome. *Crit Care Med* 2015;43:1790–1797.
8. Hsieh SJ, Zhuo H, Benowitz NL, Thompson BT, Liu KD, Matthay MA, Calfee CS; National Heart, Lung, and Blood Institute Acute Respiratory Distress Syndrome Network; National Heart Lung and Blood Institute Acute Respiratory Distress Syndrome Network. Prevalence and impact of active and passive cigarette smoking in acute respiratory distress syndrome. *Crit Care Med* 2014;42:2058–2068.
9. Iribarren C, Jacobs DR Jr, Sidney S, Gross MD, Eisner MD. Cigarette smoking, alcohol consumption, and risk of ARDS: a 15-year cohort study in a managed care setting. *Chest* 2000;117: 163–168.
10. Ho KM, Hart G, Austin D, Hunter M, Botha J, Chavan S. Dose-related effect of smoking on mortality in critically ill patients: a multicentre cohort study. *Intensive Care Med* 2011;37:981–989.
11. Mercado N, Thimmulappa R, Thomas CM, Fenwick PS, Chana KK, Donnelly LE, Biswal S, Ito K, Barnes PJ. Decreased histone deacetylase 2 impairs Nrf2 activation by oxidative stress. *Biochem Biophys Res Commun* 2011;406:292–298.
12. Rajendrasozhan S, Yao H, Rahman I. Current perspectives on role of chromatin modifications and deacetylases in lung inflammation in COPD. *COPD* 2009;6:291–297.
13. Yao H, Rahman I. Role of histone deacetylase 2 in epigenetics and cellular senescence: implications in lung inflammaging and COPD. *Am J Physiol Lung Cell Mol Physiol* 2012;303: L557–L566.
14. Burns AR, Hosford SP, Dunn LA, Walker DC, Hogg JC. Respiratory epithelial permeability after cigarette smoke exposure in guinea pigs. *J Appl Physiol (1985)* 1989;66:2109–2116.
15. Maini CL, Bonetti MG, Giordano A, Pistelli R, Antonelli Incalzi R, Marchetti L. Dynamic pulmonary scintigraphy with Tc99m radioaerosol for the evaluation of the permeability of the alveolo-capillary barrier [in Italian]. *Radiol Med (Torino)* 1987;74: 520–524.
16. O'Brodovich H, Coates G. Pulmonary clearance of 99mTc-DTPA: a noninvasive assessment of epithelial integrity. *Lung* 1987;165:1–16.
17. Hirsch J, Chalkley RJ, Bentley T, Burlingame AL, Frank JA. Double impact of cigarette smoke and mechanical ventilation on the alveolar epithelial type II cell. *Crit Care* 2014;18:R50.
18. Ozaki K, Hori T, Ishibashi T, Nishio M, Aizawa Y. Effects of chronic cigarette smoking on endothelial function in young men. *J Cardiol* 2010;56:307–313.
19. Ferrer E, Peinado VI, Díez M, Carrasco JL, Musri MM, Martínez A, Rodríguez-Roisin R, Barberà JA. Effects of cigarette smoke on endothelial function of pulmonary arteries in the guinea pig. *Respir Res* 2009;10:76.
20. Wright JL, Churg A. Short-term exposure to cigarette smoke induces endothelial dysfunction in small intrapulmonary arteries: analysis using guinea pig precision cut lung slices. *J Appl Physiol (1985)* 2008;104:1462–1469.
21. Barberà JA, Blanco I. Pulmonary hypertension in patients with chronic obstructive pulmonary disease: advances in pathophysiology and management. *Drugs* 2009;69:1153–1171.
22. Peinado VI, Pizarro S, Barberà JA. Pulmonary vascular involvement in COPD. *Chest* 2008;134:808–814.
23. Barberà JA. Mechanisms of development of chronic obstructive pulmonary disease-associated pulmonary hypertension. *Pulm Circ* 2013;3:160–164.
24. Holden WE, Maier JM, Malinow MR. Cigarette smoke extract increases albumin flux across pulmonary endothelium *in vitro*. *J Appl Physiol (1985)* 1989;66:443–449.
25. Lu Q, Sakhatskyy P, Grinnell K, Newton J, Ortiz M, Wang Y, Sanchez-Esteban J, Harrington EO, Rounds S. Cigarette smoke causes lung vascular barrier dysfunction via oxidative stress–mediated inhibition of RhoA and focal adhesion kinase. *Am J Physiol Lung Cell Mol Physiol* 2011;301:L847–L857.
26. Schweitzer KS, Hatoum H, Brown MB, Gupta M, Justice MJ, Beteck B, Van Demark M, Gu Y, Presson RG Jr, Hubbard WC, *et al*. Mechanisms of lung endothelial barrier disruption induced by cigarette smoke: role of oxidative stress and ceramides. *Am J Physiol Lung Cell Mol Physiol* 2011;301:L836–L846.
27. Bazin M, Turcotte H, Lagacé R, Boutet M. Cardiovascular effects of cigarette smoke in the rat. Aortic endothelial and myocardial capillary permeability in the rat [in French]. *Rev Can Biol* 1981;40:263–276.
28. Dejana E, Orsenigo F, Lampugnani MG. The role of adherens junctions and VE-cadherin in the control of vascular permeability. *J Cell Sci* 2008;121:2115–2122.
29. Taddei A, Giampietro C, Conti A, Orsenigo F, Breviario F, Pirazzoli V, Potente M, Daly C, Dimmeler S, Dejana E. Endothelial adherens junctions control tight junctions by VE-cadherin–mediated upregulation of claudin-5. *Nat Cell Biol* 2008;10:923–934.

30. Petrache I, Birukova A, Ramirez SI, Garcia JG, Verin AD. The role of the microtubules in tumor necrosis factor-α–induced endothelial cell permeability. *Am J Respir Cell Mol Biol* 2003;28:574–581.
31. van Buul JD, Anthony EC, Fernandez-Borja M, Burridge K, Hordijk PL. Proline-rich tyrosine kinase 2 (Pyk2) mediates vascular endothelial-cadherin–based cell–cell adhesion by regulating beta-catenin tyrosine phosphorylation. *J Biol Chem* 2005;280: 21129–21136.
32. Li Y, Zhang X, Polakiewicz RD, Yao TP, Comb MJ. HDAC6 is required for epidermal growth factor–induced β-catenin nuclear localization. *J Biol Chem* 2008;283:12686–12690.
33. Dudek SM, Jacobson JR, Chiang ET, Birukov KG, Wang P, Zhan X, Garcia JG. Pulmonary endothelial cell barrier enhancement by sphingosine 1-phosphate: roles for cortactin and myosin light chain kinase. *J Biol Chem* 2004;279:24692–24700.
34. Wu H, Reynolds AB, Kanner SB, Vines RR, Parsons JT. Identification and characterization of a novel cytoskeleton-associated pp60src substrate. *Mol Cell Biol* 1991;11:5113–5124.
35. Birukova AA, Birukov KG, Smurova K, Adyshev D, Kaibuchi K, Alieva I, Garcia JG, Verin AD. Novel role of microtubules in thrombin-induced endothelial barrier dysfunction. *FASEB J* 2004;18:1879–1890.
36. Mirzapoiazova T, Kolosova IA, Moreno L, Sammani S, Garcia JG, Verin AD. Suppression of endotoxin-induced inflammation by taxol. *Eur Respir J* 2007;30:429–435.
37. Verin AD, Birukova A, Wang P, Liu F, Becker P, Birukov K, Garcia JG. Microtubule disassembly increases endothelial cell barrier dysfunction: role of MLC phosphorylation. *Am J Physiol Lung Cell Mol Physiol* 2001;281:L565–L574.
38. Bernhard D, Csordas A, Henderson B, Rossmann A, Kind M, Wick G. Cigarette smoke metal–catalyzed protein oxidation leads to vascular endothelial cell contraction by depolymerization of microtubules. *FASEB J* 2005;19:1096–1107.
39. Hubbert C, Guardiola A, Shao R, Kawaguchi Y, Ito A, Nixon A, Yoshida M, Wang XF, Yao TP. HDAC6 is a microtubule-associated deacetylase. *Nature* 2002;417:455–458.
40. Lam HC, Cloonan SM, Bhashyam AR, Haspel JA, Singh A, Sathirapongsasuti JF, Cervo M, Yao H, Chung AL, Mizumura K, *et al*. Histone deacetylase 6–mediated selective autophagy regulates COPD-associated cilia dysfunction. *J Clin Invest* 2013; 123:5212–5230.
41. Demos-Davies KM, Ferguson BS, Cavasin MA, Mahaffey JH, Williams SM, Spiltoir JI, Schuetze KB, Horn TR, Chen B, Ferrara C, *et al*. HDAC6 contributes to pathological responses of heart and skeletal muscle to chronic angiotensin-II signaling. *Am J Physiol Heart Circ Physiol* 2014;307:H252–H258.
42. Govindarajan N, Rao P, Burkhardt S, Sananbenesi F, Schlüter OM, Bradke F, Lu J, Fischer A. Reducing HDAC6 ameliorates cognitive deficits in a mouse model for Alzheimer's disease. *EMBO Mol Med* 2013;5:52–63.
43. Xiong Y, Zhao K, Wu J, Xu Z, Jin S, Zhang YQ. HDAC6 mutations rescue human tau-induced microtubule defects in *Drosophila*. *Proc Natl Acad Sci USA* 2013;110:4604–4609.
44. Fukada M, Hanai A, Nakayama A, Suzuki T, Miyata N, Rodriguiz RM, Wetsel WC, Yao TP, Kawaguchi Y. Loss of deacetylation activity of Hdac6 affects emotional behavior in mice. *PLoS One* 2012;7: e30924.
45. Jochems J, Boulden J, Lee BG, Blendy JA, Jarpe M, Mazitschek R, Van Duzer JH, Jones S, Berton O. Antidepressant-like properties of novel HDAC6-selective inhibitors with improved brain bioavailability. *Neuropsychopharmacology* 2014;39:389–400.
46. Winkler R, Benz V, Clemenz M, Bloch M, Foryst-Ludwig A, Wardat S, Witte N, Trappiel M, Namsolleck P, Mai K, *et al*. Histone deacetylase 6 (HDAC6) is an essential modifier of glucocorticoid-induced hepatic gluconeogenesis. *Diabetes* 2012;61:513–523.
47. Krämer OH, Mahboobi S, Sellmer A. Drugging the HDAC6–HSP90 interplay in malignant cells. *Trends Pharmacol Sci* 2014;35: 501–509.
48. Saito S, Lasky JA, Guo W, Nguyen H, Mai A, Danchuk S, Sullivan DE, Shan B. Pharmacological inhibition of HDAC6 attenuates endothelial barrier dysfunction induced by thrombin. *Biochem Biophys Res Commun* 2011;408:630–634.
49. Ni YF, Wang J, Yan XL, Tian F, Zhao JB, Wang YJ, Jiang T. Histone deacetylase inhibitor, butyrate, attenuates lipopolysaccharide-induced acute lung injury in mice. *Respir Res* 2010;11:33.
50. Zhang Y, Kwon S, Yamaguchi T, Cubizolles F, Rousseaux S, Kneissel M, Cao C, Li N, Cheng HL, Chua K, *et al*. Mice lacking histone deacetylase 6 have hyperacetylated tubulin but are viable and develop normally. *Mol Cell Biol* 2008;28: 1688–1701.
51. Chattopadhyay S, Fensterl V, Zhang Y, Veleeparambil M, Wetzel JL, Sen GC. Inhibition of viral pathogenesis and promotion of the septic shock response to bacterial infection by IRF-3 are regulated by the acetylation and phosphorylation of its coactivators. *MBio* 2013;4:pii: e00636-12.
52. Kaluza D, Kroll J, Gesierich S, Yao TP, Boon RA, Hergenreider E, Tjwa M, Rössig L, Seto E, Augustin HG, *et al*. Class IIb HDAC6 regulates endothelial cell migration and angiogenesis by deacetylation of cortactin. *EMBO J* 2011;30:4142–4156.
53. Zhang X, Yuan Z, Zhang Y, Yong S, Salas-Burgos A, Koomen J, Olashaw N, Parsons JT, Yang XJ, Dent SR, *et al*. HDAC6 modulates cell motility by altering the acetylation level of cortactin. *Mol Cell* 2007;27:197–213.
54. Stevens TC, Ochoa CD, Morrow KA, Robson MJ, Prasain N, Zhou C, Alvarez DF, Frank DW, Balczon R, Stevens T. The *Pseudomonas aeruginosa* exoenzyme Y impairs endothelial cell proliferation and vascular repair following lung injury. *Am J Physiol Lung Cell Mol Physiol* 2014;306:L915–L924.
55. Lu Q, Harrington EO, Newton J, Casserly B, Radin G, Warburton R, Zhou Y, Blackburn MR, Rounds S. Adenosine protected against pulmonary edema through transporter- and receptor A2–mediated endothelial barrier enhancement. *Am J Physiol Lung Cell Mol Physiol* 2010;298:L755–L767.
56. Lu Q, Harrington EO, Hai C-M, Newton J, Garber M, Hirase T, Rounds S. Isoprenylcysteine carboxyl methyltransferase modulates endothelial monolayer permeability: involvement of RhoA carboxyl methylation. *Circ Res* 2004;94:306–315.
57. Lu Q, Harrington EO, Jackson H, Morin N, Shannon C, Rounds S. Transforming growth factor-beta1–induced endothelial barrier dysfunction involves Smad2-dependent p38 activation and subsequent RhoA activation. *J Appl Physiol (1985)* 2006;101:375–384.
58. Ochoa CD, Stevens T, Balczon R. Cold exposure reveals two populations of microtubules in pulmonary endothelia. *Am J Physiol Lung Cell Mol Physiol* 2011;300:L132–L138.
59. Haggarty SJ, Koeller KM, Wong JC, Grozinger CM, Schreiber SL. Domain-selective small-molecule inhibitor of histone deacetylase 6 (HDAC6)–mediated tubulin deacetylation. *Proc Natl Acad Sci USA* 2003;100:4389–4394.
60. Kaidanovich O, Eldar-Finkelman H. The role of glycogen synthase kinase-3 in insulin resistance and type 2 diabetes. *Expert Opin Ther Targets* 2002;6:555–561.
61. Chen S, Owens GC, Makarenkova H, Edelman DB. HDAC6 regulates mitochondrial transport in hippocampal neurons. *PLoS One* 2010;5: e10848.
62. Ware LB, Lee JW, Wickersham N, Nguyen J, Matthay MA, Calfee CS; California Transplant Donor Network. Donor smoking is associated with pulmonary edema, inflammation and epithelial dysfunction in *ex vivo* human donor lungs. *Am J Transplant* 2014;14:2295–2302.
63. Mizumura K, Cloonan SM, Nakahira K, Bhashyam AR, Cervo M, Kitada T, Glass K, Owen CA, Mahmood A, Washko GR, *et al*. Mitophagy-dependent necroptosis contributes to the pathogenesis of COPD. *J Clin Invest* 2014;124:3987–4003.
64. Zhang L, Jin S, Wang C, Jiang R, Wan J. Histone deacetylase inhibitors attenuate acute lung injury during cecal ligation and puncture–induced polymicrobial sepsis. *World J Surg* 2010;34: 1676–1683.
65. Chen HY, Li L, Fu ZJ. Histone deacetylase inhibitors trichostatin A and suberoylanilide hydroxamic acid attenuate ventilator-induced lung injury. *Pharmazie* 2014;69:55–59.
66. Wang B, Rao YH, Inoue M, Hao R, Lai CH, Chen D, McDonald SL, Choi MC, Wang Q, Shinohara ML, *et al*. Microtubule acetylation amplifies p38 kinase signalling and anti-inflammatory IL-10 production. *Nat Commun* 2014;5:3479.

67. Ito K, Ito M, Elliott WM, Cosio B, Caramori G, Kon OM, Barczyk A, Hayashi S, Adcock IM, Hogg JC, *et al*. Decreased histone deacetylase activity in chronic obstructive pulmonary disease. *N Engl J Med* 2005;352:1967–1976.
68. Lafarga V, Aymerich I, Tapia O, Mayor F Jr, Penela P. A novel GRK2/HDAC6 interaction modulates cell spreading and motility. *EMBO J* 2012;31:856–869.
69. Wang J, Lin A, Lu L. Effect of EGF-induced HDAC6 activation on corneal epithelial wound healing. *Invest Ophthalmol Vis Sci* 2010;51:2943–2948.
70. Watabe M, Nakaki T. Protein kinase CK2 regulates the formation and clearance of aggresomes in response to stress. *J Cell Sci* 2011;124:1519–1532.
71. Deribe YL, Wild P, Chandrashaker A, Curak J, Schmidt MH, Kalaidzidis Y, Milutinovic N, Kratchmarova I, Buerkle L, Fetchko MJ, *et al*. Regulation of epidermal growth factor receptor trafficking by lysine deacetylase HDAC6. *Sci Signal* 2009;2:ra84.
72. Huang X, Begley M, Morgenstern KA, Gu Y, Rose P, Zhao H, Zhu X. Crystal structure of an inactive Akt2 kinase domain. *Structure* 2003;11:21–30.
73. Hayashi I, Morishita Y, Imai K, Nakamura M, Nakachi K, Hayashi T. High-throughput spectrophotometric assay of reactive oxygen species in serum. *Mutat Res* 2007;631:55–61.
74. Durgadoss L, Nidadavolu P, Valli RK, Saeed U, Mishra M, Seth P, Ravindranath V. Redox modification of Akt mediated by the dopaminergic neurotoxin MPTP, in mouse midbrain, leads to down-regulation of pAkt. *FASEB J* 2012;26:1473–1483.
75. Kim SY, Lee JH, Huh JW, Ro JY, Oh YM, Lee SD, An S, Lee YS. Cigarette smoke induces Akt protein degradation by the ubiquitin–proteasome system. *J Biol Chem* 2011;286:31932–31943.
76. Matsuyama A, Shimazu T, Sumida Y, Saito A, Yoshimatsu Y, Seigneurin-Berny D, Osada H, Komatsu Y, Nishino N, Khochbin S, *et al*. *In vivo* destabilization of dynamic microtubules by HDAC6-mediated deacetylation. *EMBO J* 2002;21:6820–6831.
77. Zhang Y, Li N, Caron C, Matthias G, Hess D, Khochbin S, Matthias P. HDAC-6 interacts with and deacetylates tubulin and microtubules *in vivo*. *EMBO J* 2003;22:1168–1179.